Clays and Clay Minerals, Vol. 54, No. 5, 541–554, 2006.

CLAY MINERALS FORMED DURING PROPYLITIC ALTERATION OF A GRANITE AND THEIR INFLUENCE ON PRIMARY POROSITY: A MULTI-SCALE APPROACH

M. Cassiaux[1], D. Proust[1,*], M. Siitari-Kauppi[2], P. Sardini[1] and Y. Leutsch[3]

[1] UMR 6532 CNRS, HydrASA, Faculté des Sciences, 40 Avenue du recteur Pineau, 86022 Poitiers cedex, France
[2] Laboratory of Radiochemistry, Department of Chemistry, PO Box 55, FIN-00014, University of Helsinki, Finland
[3] ANDRA, Parc de la Croix Blanche, 1/7 rue Jean Monnet, 92290 Chatenay-Malabry, France

Abstract—The porosity of a propylitized granite from Charroux (France), with no fractures or sealed fractures, increases by more than four times from the unaltered (0.3%) to the altered rock (1.4%). This evolution results from several local porosity modifications which occur at different scales in the rock: (1) at the core scale, from 10^{-1} to 10^{-5} m, where rock porosity changes as a function of rock-forming mineralogical composition; (2) at the mineral scale, from 10^{-3} to 10^{-7} m, where porosity depends both on the nature of the rock-forming mineral and its clay mineral alteration. Mineralogical and porosity data collected from the granite using a mineralogical map (after chemical staining and scanning electron microscopy images combined with autoradiographs) indicate that (1) the ferromagnesian rock-forming minerals – biotite and magnesiohornblende – act as the main porosity source in the unaltered granite, and (2) the nature of the clay minerals replacing rock-forming minerals in the altered granite appears to control the porosity value through two major alteration processes: chloritization and phengitization which affect the ferromagnesian minerals and produce non-porous chloritic and porous phengitic areas, respectively, at the studied scales. The observation that incipient porosity formation in granites is strongly linked to the pathway of ferromagnesian silicate alteration and subsequent clay mineral formation underlines the need to study parent-rock texture and mineralogy and their effects on subsequent near-surface weathering of granites.

Key Words—Autoradiograph, Connected Porosity, Granite, Microprobe Analysis, Propylitic Alteration, SEM, XRD.

INTRODUCTION

Whatever the origin of rock alteration, it is driven by fluid-rock interactions where temperature, fluid chemistry, mineral species, rock texture and rate of fluid flow are the major parameters. These interactions can operate over a wide range of time and are strongly influenced by the fluid pathway patterns, from nm to km scale. In this way, the connected porosity and its evolution inside the rock have to be considered as important physical parameters in the study of alteration processes. The observation of the connected porous patterns in a rock reveals various fluid pathway morphologies: intergranular and intragranular pores, grain boundaries, cracks and fractures that can be simultaneously observed in the same rock and may have different influence on the fluid flow and fluid-rock interactions.

The bulk connected porosity measured in a given rock appears then as the sum of connected porosities within specific microsites which have to be identified, described and measured both at the scale of the rock and at the scale of the minerals. Previous work on fluid-rock interactions in igneous rocks highlights two different but complementary ways of studying porosity depending on whether or not the mineralogical heterogeneity of the rock is considered. Bulk porosity is measured by the water-porosity impregnation method (Melnyk and Skeet, 1986). Results can be improved by considering the pore size obtained with mercury porosity (Geraud *et al.*, 1992; Hellmuth *et al.*, 1999) and the porous network geometry revealed by electrical conductivity (Revil and Glover, 1997).

The need to consider the mineralogical heterogeneity of the rock in smaller-scale porosity studies was strengthened by numerous rock-alteration studies which revealed: (1) the crystallochemical nature of a given rock-forming mineral strongly influences the size and the geometry of the porous network which develops inside the crystal; (2) each rock-forming mineral produces specific alteration phases and associated porosity; and (3) a modification of the connected porous network. Effects include: (a) porosity generation during mineral replacement (Walker *et al.*, 1995; Ferry, 2000; Putnis, 2002); (b) fracture or crack sealing by clay mineral recrystallization (Vaughan *et al.*, 1986); (c) crack network opening by dissolution processes (Saussse *et al.*, 2001); and (d) new fracture generation by clay mineral swelling (Suzuki *et al.*, 1998). These results gave rise to integrated works coupling two-dimensional (2D) or three-dimensional (3D)

* E-mail address of corresponding author:
dominique.proust@hydrasa.univ-poitiers.fr
DOI: 10.1346/CCMN.2006.0540502

geometry studies in order to correlate the porous network with the mineralogical rock composition at various observation scales: (1) 2D decimetre scale using ^{14}C-PMMA impregnation method associated with autoradiograph films and optical digital image-processing techniques (Hellmuth *et al.*, 1993, 1994; Siitari-Kauppi, 2002); (2) 2D microscopic scale using scanning electron microscopy (SEM) (Montgomery and Brace, 1975) or ion probe microanalysis (David and Walker, 1990); (3) 3D microscopic scale using confocal scanning laser microscopy (Montoto *et al.*, 1995; Fredrich and Lindquist, 1997); (4) X-ray tomography (Geraud *et al.*, 1998; Duliu, 1999; Karacan *et al.*, 2003).

These studies, however, were essentially focused on fluid pathways in deformed or fractured rocks without considering the specific porosity of each rock-forming mineral and its specific alteration products. This study was thus planned to get better insight into the development of the matrix porosity during granite alteration at different scales as a function of (1) the rock-forming mineral species and (2) the nature of their specific alteration phases.

MATERIALS AND METHODS

Materials

This work is focused on the granitic body from the Charroux-Civray granitoid complex (western France) with an age of 355±5 Ma (Bertrand *et al.*, 2001) that is modified by a fissural and pervasive propylitic alteration of Hercynian age (Freiberger, 2000). Two samples were collected from the CHA 106 borehole: a core of unaltered granite collected at 248.30 m depth and a core of altered granite close to a fracture collected at a depth of 267.90 m.

Methods

Connected porosity and mineralogy at the core scale. The bulk-rock porosity was measured by the water porosity impregnation method of Melnyk and Skeet (1986) which is currently used for rocks with low porosity (<5%) and produces 0.2% as the relative error. This method does not use sample drying with a wet cloth, and hence does not overestimate the saturated mass sample. The correlation between porosity and rock mineralogy was examined after rock impregnation with methyl methacrylate doped with ^{14}C (^{14}C-MMA) to obtain a porosity map and after chemical staining of minerals to obtain a mineralogical map. The granite core was impregnated as a whole with the ^{14}C-MMA under primary vacuum, prior to slicing to produce a planar internal surface. This method ensures that the porosity measured by autoradiography is really 3D connected although visualized on a 2D film. The ^{14}C-MMA resin was polymerized into poly-methyl methacrylate (^{14}C-PMMA) after 4 days' exposure to a ^{60}Co source. The rocks were then heated at 120ºC for 3 h to avoid the primary mineral luminescence which can cause artefacts as darkening on the autoradiograph (Siitari-Kauppi, 2002). The two cores were sliced transversely and polished planar surfaces were placed on an autoradiographic film Biomax MR (Kodak) for 7 days. The gray levels were normalized using calibration standards prepared from ^{14}C-PMMA exposed simultaneously with the cores. The theoretical film resolution is a few microns, but the apparent image resolution depends on (1) the beta emitter used for irradiation: 20 μm for ^{14}C emitters from the rock source; and (2) the distance between the sample and the film which is controlled by the polishing quality of the analyzed surface: when the distance between the sample and the film reaches 3 μm, the apparent image resolution decreases to 85 μm (Siitari-Kauppi *et al.*, 1998). The autoradiographs were scanned using a flatbed scanner at 600 dpi resolution giving 42.5 μm as the pixel size. As a consequence, the local porosity calculated for each pixel by comparison with calibration standards would correspond to a zone 42.5 μm wide.

The mineralogical maps of the autoradiographed surfaces were obtained by mineral-staining processes. The ferromagnesian minerals were first stained in blue with a solution of HCl and Na ferrocyanid (Müller, 1967). The feldspars, when free of ferromagnesian minerals, are not affected by this blue coloration. The next step was the etching of mineral surfaces by HF to prepare the feldspar coloration. K-feldspars were then stained yellow by contact with Na-cobaltinitrite solution, Ca-Na plagioclases pink with amaranth solution. Albite remained white. For each staining step, etched surfaces were scanned in 24-bit RGB mode using the same flatbed scanner and resolution as the autoradiographs (600 dpi) and minerals were identified using a thresholding procedure applied simultaneously to the three color components of each pixel (Sardini *et al.*, 1999). Finally, the superposition of the autoradiograph and mineralogical maps allowed us to correlate the measured connected porosity with each mineral group, *i.e.* to define the mineral-specific porosity. The distribution of the specific porosity within each mineral group is illustrated in frequency diagrams (*e.g.* Figure 3) where the horizontal axis is the porosity % as defined by the gray levels in calibration standards and the vertical axis corresponds to the number of pixels counted in each mineral-specific porosity class divided by the total number of pixels describing the mineral group. This allows us to compare the mineral porosity distribution whatever the modal composition of the rock and thus to follow the porosity evolution at different alteration stages. However, the scanning resolution (pixel size 42.5 μm) did not allow detection of the alteration phases. This problem was solved by a petrographic study of the alteration phases at the thin-section scale to correlate more precisely the alteration processes with the connected porosity.

https://doi.org/10.1346/CCMN.2006.0540502 Published online by Cambridge University Press

Connected porosity and mineralogy at the mineral scale. Thin-sections were prepared from impregnated cores and autoradiographed to obtain a porosity map. According to Beer's Law, the beta radiation intensity decreases to zero at a depth of 50 μm from the surface of common silicates (Sammartino *et al.*, 2001; Siitari-Kauppi, 2002). This implies that, with 30 μm thin-sections, the porosity information between 30 and 50 μm will be missing when compared to the cores. This corresponded to ~20% of the porosity. The chemical staining differentiated the feldspars but did not separate amphibole from biotite within the ferromagnesian minerals. To improve mineralogical identification, the amphiboles and biotites were located by optical means on scanned thin-sections and correlated with the autoradiographs to calculate their porosities. Primary mineral species and their corresponding alteration phases were separated with regards to their porosity and analyzed chemically. Chemical data were obtained using a CAMECA SX 50 electron microprobe (WDS analysis) at the 'Service d'analyse CAMPARIS' at the University of Paris VI. The analytical conditions were as follows: accelerating voltage of 15 kV, beam size of 1 μm, beam current of 4 nA, counting time of 10 s for each analyzed element.

Primary minerals and their alteration phases were also identified using X-ray diffraction (XRD). Minerals were extracted from the thin-sections with an ultrasonic probe to obtain powdered preparations. The XRD patterns were recorded from random powdered and oriented preparations using a Philips PW 1730 diffractometer (40 kV, 40 mA) with Fe-filtered CoKα radiation and a stepping motor-driven goniometer with a DACO-MP recorder using the Diffrac-AT software (Socabim). Thin-sections were carbon coated for SEM examination by a JEOL JSM 5600-LV scanning electron microscope in backscattered electron mode to determine the porosity network at a higher magnification.

RESULTS

Connected porosity and mineralogy at the core scale

Bulk porosity and mineralogical map. The bulk connected porosity measured in the unaltered granite with the ^{14}C-PMMA method (Figure 1a) was 0.2%±0.1%, in good agreement with the porosity value obtained by the water impregnation method (0.3%±0.2%). The ^{14}C-PMMA porosity measured in the altered granite shows exponential evolution as a function of the distance to the fracture (Figure 1b,c), with a general decrease from 4.0% at the fracture wall to 0.2% in the rock, 5 cm from the fracture surface, a value comparable to that in the unaltered granite. The modal composition (area%) of the unaltered granite obtained from point counting gives 21% K-feldspars, 42% plagioclase phenocryts in a matrix of 24% quartz, 11% biotite and 6% hornblende, whereas the composition obtained from the mineralogical map gives 21% K-feldspars, 44% plagioclase phenocryts, 23% quartz, 12% biotite and hornblende. The largest discrepancy between the two methods is observed when counting ferromagnesian minerals (5%). Most primary mineral grains are ~6 mm in length but some feldspar phenocrysts can reach 10 mm.

Biotite and hornblende cannot be distinguished on the mineralogical map because of their similar and homogeneous stained colorations both in unaltered and altered granite cores (Figure 2a,b). The homogeneous stained pink coloration of plagioclases in the unaltered granite is somewhat different in the altered granite where three alteration zones can be observed on the basis of the plagioclase color (Figure 2c) and the chemical composition of their alteration phases (albite and phengite in Table 4): zone 1 close to the fracture selvage with light blue plagioclases indicative of their replacement by a mixture of albite and ferromagnesian minerals, zone 2 where white colored plagioclases are indicative of their complete albitization, and zone 3 with partially pink colored plagioclases, farthest from the fracture surface, which imply their partial albitization.

Porosity measurement of each mineral group. The specific porosity of each rock-forming mineral group (Table 1) and its distribution into unaltered and altered granite are illustrated in Figure 3a,b. The porosities of quartz and K-feldspars in the unaltered granite are very low, 0.2% and 0.1%, respectively. They are of the same magnitude as the other rock-forming minerals and do not increase in a significant manner in the altered granite. The increase in porosity for K-feldspar is within the uncertainty of the measurement (relative error ~0.1%), whereas porosity increase in quartz is overestimated due to artefacts during image analysis, because pixels which have not been thresholded as porous feldspars or ferromagnesian minerals are assigned to quartz. These pixels might be porous secondary minerals that cannot be differentiated or porous ferromagnesian minerals smaller than the resolution of the mineralogical map. The specific porosity of the ferromagnesian minerals increases from 0.4 to 3.7% with alteration (Table 1) and exhibits great variability ranging from a 0.7% maximum porosity value

Table 1. Bulk-rock and mineral-specific porosities in unaltered and altered granite.

	Unaltered granite (%)	Altered granite (%)
Bulk rock	0.2	1.4
Quartz	0.2	0.8
Fe-Mg minerals	0.4	3.7
K-feldspar	0.1	0.3
Plagioclase	0.1	2.2
Zone 1: blue plagioclase	–	3.7
Zone 2: white plagioclase	–	1.6
Zone 3: pink plagioclase	–	0.7

https://doi.org/10.1346/CCMN.2006.0540502 Published online by Cambridge University Press

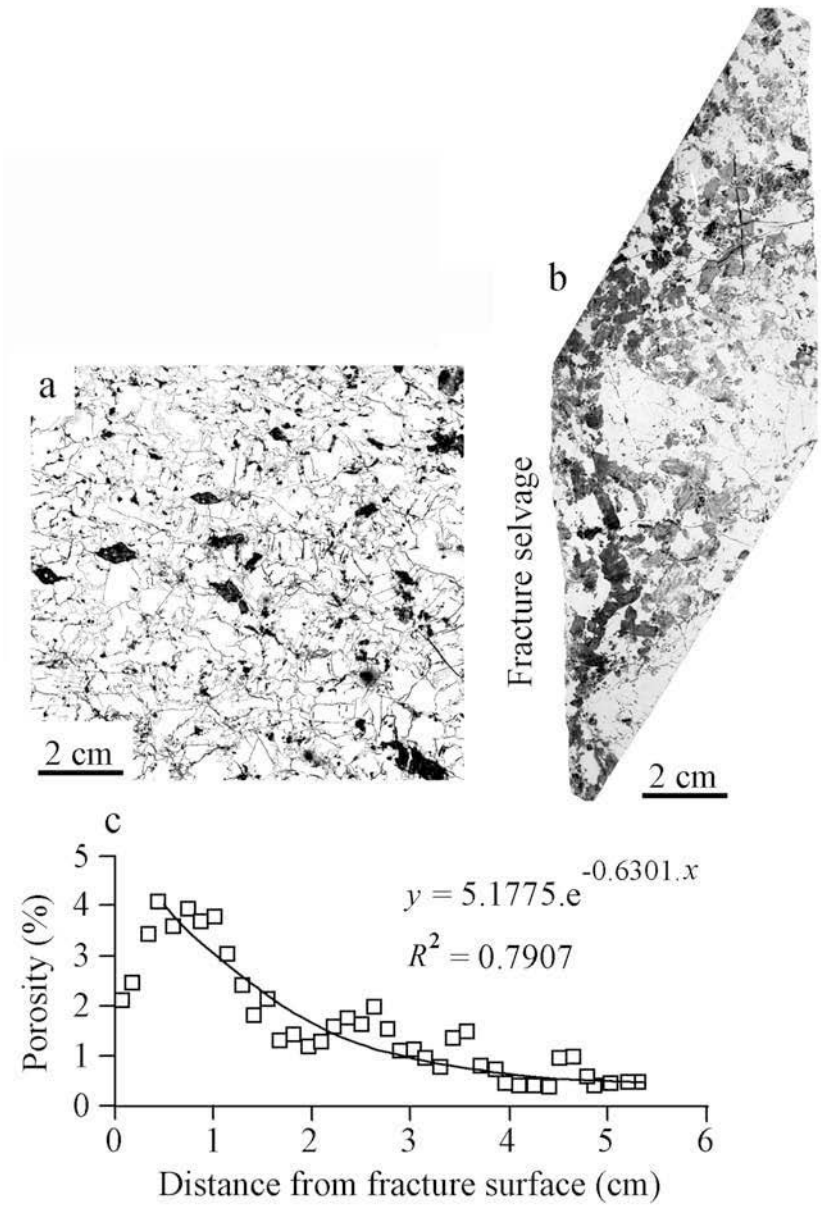

Figure 1. (a) Autoradiograph of the unaltered granite; (b) autoradiograph of the altered granite. The darker the shade, the greater the degree of connected porosity; (c) porosity profile of the altered granite as a function of the distance from the fracture selvage. The exponential fitting curve gives a rough idea of the porosity evolution in the altered sample; the first 2 mm are not considered due to ^{14}C-MMA out-leaching during the resin polymerization.

in the unaltered to 20% in the altered granite. However, 4.8% of ferromagnesian minerals produce saturated pixels on the autoradiograph which are not considered in the porosity calculation. As a consequence, ferromagnesian mineral-specific porosity is under-evaluated because of film saturation. The porosity of the plagioclases displays the same behavior as that of ferromagnesian minerals, increasing from 0.1% in the unaltered to 2.2% in the altered granite. The three alteration zones recognized from plagioclase staining colors on the mineralogical map are differentiated by their plagioclase specific-porosity values, 3.7%, 1.6% and 0.7% for alteration zones 1, 2 and 3, respectively (Figure 3c). The ferromagnesian minerals and the plagioclases are the major mineral species responsible for the increase in porosity in the granite.

Connected porosity and mineralogy at the mineral scale.

Mineralogy and porosity of amphiboles. The amphiboles of the unaltered granite appear as euhedral prismatic crystals, up to 6 mm long with slightly inclined (<30º) extinction, high relief and light- to dark-green pleochro-

https://doi.org/10.1346/CCMN.2006.0540502 Published online by Cambridge University Press

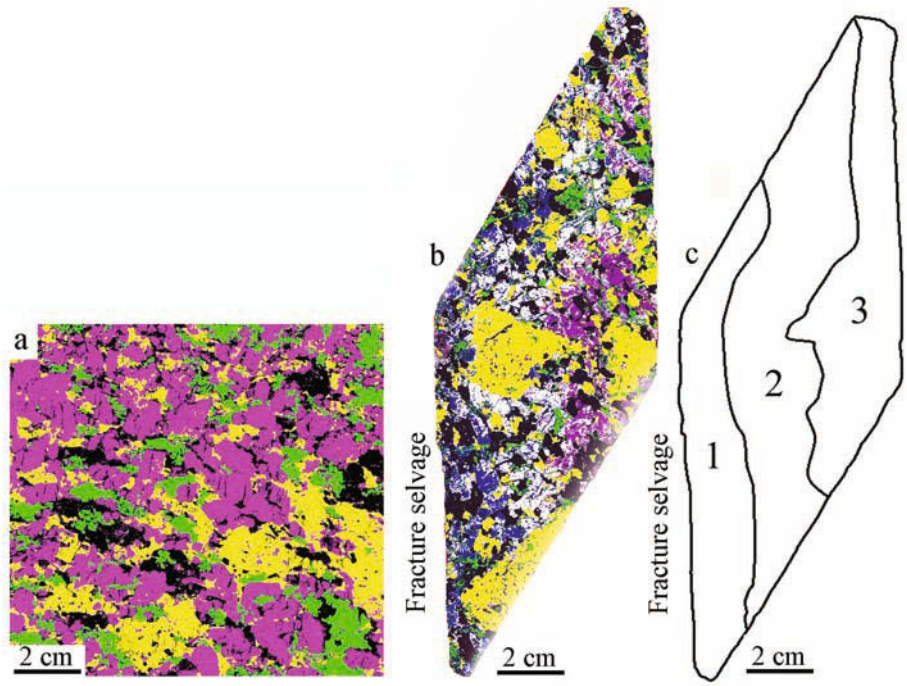

Figure 2. (a) Mineralogical map of the unaltered granite. The color code is green for ferromagnesian minerals (amphiboles and Fe-Mg micas), yellow for K-feldspars, pink for unaltered plagioclases and black for quartz; (b) Mineralogical map of the altered granite. The color code is the same as (a) with altered plagioclases appearing in blue for alteration zone 1, white for alteration zone 2, purple for alteration zone 3 (see Figure 2c); (c) sketch of the three alteration zones shown by the staining method in the altered core.

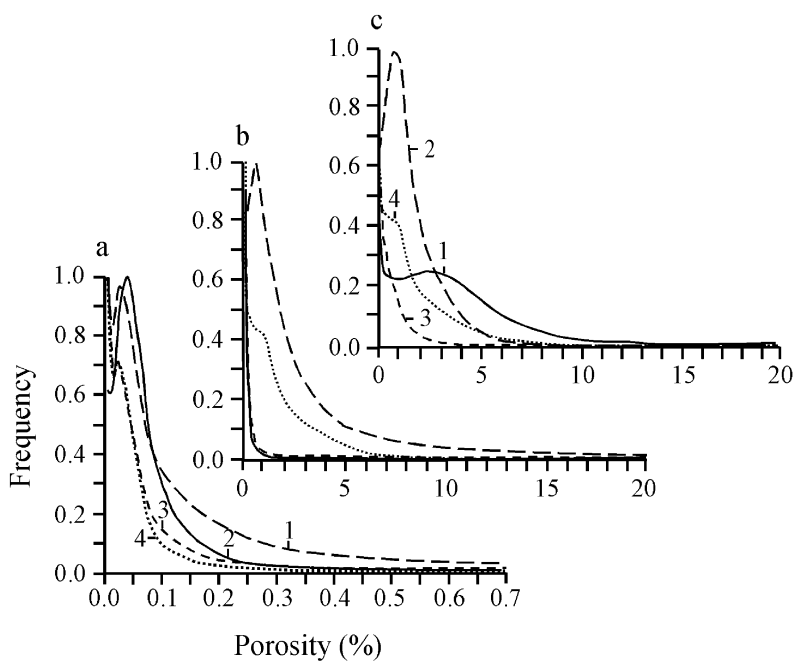

Figure 3. Mineral-specific porosity distribution in (a) unaltered and (b) altered granite. 1 = ferromagnesian minerals, 2 = K-feldspars, 3 = quartz, 4 = plagioclases. (c) Specific porosity distribution of altered plagioclases in the three alteration zones (see Figure 2c). 1 = altered plagioclases in zone 1, 2 = altered plagioclases in zone 2, 3 = altered plagioclases in zone 3, 4 = altered plagioclases in whole sample (zone 1 + zone 2 + zone 3); the *y* scales in (a), (b) and (c) correspond to the number of pixels observed within each mineral-specific porosity class divided by the maximum pixel value obtained for each mineral group. This allows us to compare the mineral porosity distribution whatever the modal composition.

https://doi.org/10.1346/CCMN.2006.0540502 Published online by Cambridge University Press

ism under plane-polarized light. Their powder XRD patterns (Figure 4a, pattern 1) show four strong reflections, 020−110 at 9.05−8.45 Å and 240−310 at 3.29−3.14 Å, associated with additional reflections at 4.55, 3.40 and 2.95 Å which are distinctive of a magnesiohornblende. Weak reflections at 14.28, 7.12, 4.73 and 3.55 Å can be attributed to chlorite whereas apatite and calcite are identified by their 2.71−2.81 Å and 3.03 Å reflections, respectively. These minerals, however, appear as very minute inclusions in the crystals, and do not result from a major pervasive alteration of amphiboles. The chemical compositions (Table 2) are charac-

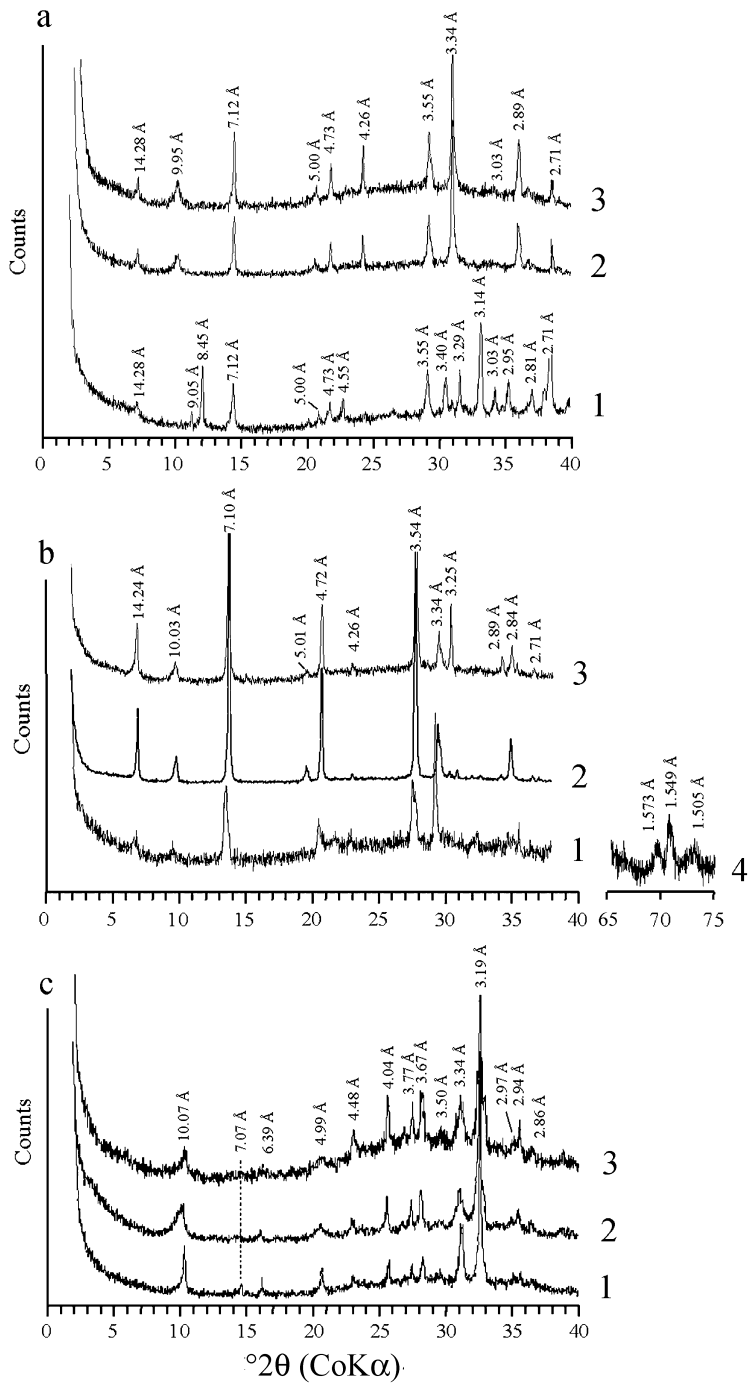

Figure 4. XRD patterns of (a) amphiboles and their alteration products, (b) biotites and their alteration products, (c) plagioclases and their alteration products. 1 = random powder XRD pattern, 2 = air-dried oriented XRD pattern, 3 = ethylene-glycol oriented XRD pattern, 4 = random powder XRD pattern in the 060 reflection angular range.

https://doi.org/10.1346/CCMN.2006.0540502 Published online by Cambridge University Press

teristic of a magnesiohornblende with Si contents and Mg/(Mg+Fe) ratios ranging from 6.69 to 6.78 atoms and 0.51–0.55, respectively (Leake *et al.*, 1978). The chlorites belong to the clinochlore chemical domain with Fe/(Fe+Mg) ratios in the range 0.36–0.37 and Si contents ranging from 2.91 to 3.01 atoms.

The porosity observed in the amphiboles from unaltered granite is illustrated by the autoradiograph of Figure 5b and compared to the corresponding optical microscopy and SEM images of Figures 5a and 5c. The core of the amphibole crystal (Amp. in Figure 5) appears as a non-porous zone with white to very low gray level; similar gray levels are also observed where amphibole is replaced by clinochlore chlorite (Chl. in Figure 5); therefore, partial chloritization of amphibole does not produce a porous area with connected porosity. The only connected porosity observed on the autoradiograph is constituted by open amphibole cleavages with apertures ranging from 0.1 μm to 2.5 μm which produces black patches (A–c in Figure 5).

The alteration of amphiboles results in the precipitation or growth of phyllosilicates either as (1) pseudomorphic replacement of amphibole or (2) as intramineral microfracture linings with 0.1–2.5 μm apertures and partial pore fillings with apertures up to 120 μm wide. The air-dried and ethylene glycol-solvated XRD patterns of microsampled altered amphiboles (Figure 4a, patterns 2 & 3) reveal two major alteration phases, that are (1) a chlorite with a series of basal reflections at 14.28, 7.12, 4.73, 3.55 and 2.89 Å and (2) a dioctahedral mica type (called phengite, as determined by electron microprobe analysis) with basal reflections at 9.95, 5.00 and 3.33 Å (superimposed on the 3.34 Å quartz reflection). Trace amounts of apatite, calcite and quartz are revealed by their most intense 2.71, 3.03 and 4.26–3.34 Å reflections, respectively.

The chemical data (Table 2), microscopic views and PMMA autoradiographs (Figure 6a–c) illustrate the alteration products of amphibole as a function of their crystallization sites within the amphibole crystal and as a function of their distance to the fracture surface (see Figure 1b). In the altered granite far from the fracture surface, clinochlore chlorite develops as a pseudomorphic amphibole replacement. When clinochlore is compared within the amphiboles in both unaltered and altered rock, gray levels (linked directly to the connected porosity value) on each autoradiograph are similar and define alteration patches with very little or no porosity. In the selvage of the fracture, the clinochlore is replaced by chamosite (Chl. in Figure 6) with the Fe/(Fe+Mg) ratio ranging from 0.67 to 0.72 and Si contents ranging from 2.85 to 2.96 atoms (Table 2). This chamosite

Table 2. Chemical composition (wt.%) and structural formulae of amphiboles and their alteration products.

	Amphibole	Amphibole	Phengite	Phengite	Clinochlore	Clinochlore	Chamosite	Chamosite	Calcite	Calcite
Na_2O	1.40	1.34	0.08	0.48	0.20	0.18	0.10	0.28	0.20	0.16
MgO	11.16	10.62	1.65	0.41	18.53	18.53	8.26	7.82	0.45	0.51
Al_2O_3	8.36	8.81	26.83	29.84	18.96	18.39	21.92	21.17	0.05	0.08
SiO_2	44.77	44.02	45.25	43.40	28.14	28.82	27.56	25.99	0.30	0.53
K_2O	1.00	1.10	8.80	9.54	0.18	0.14	0.08	0.17	0.06	0.12
CaO	11.99	11.43	0.16	0.27	0.01	0.07	0.00	0.15	49.97	49.72
TiO_2	1.51	1.53	0.00	0.28	0.05	0.04	0.05	0.00	0.00	0.04
Cr_2O_3	0.11	0.00	0.00	0.00	0.06	0.00	0.00	0.00	0.01	0.00
MnO	0.11	0.65	0.04	0.04	0.79	0.00	1.19	1.61	0.79	0.73
NiO	0.03	0.00	0.00	0.00	0.06	0.13	0.00	0.00	0.00	0.00
FeO*	16.21	17.76	3.42	1.48	19.94	18.95	29.74	29.42	0.27	0.10
Total	97.09	97.27	86.24	85.74	86.91	85.84	88.90	86.61	52.10	51.98
	23 oxygen basis		11 oxygen basis		14 oxygen basis				1 oxygen basis	
Na	0.41	0.40	0.01	0.07	0.04	0.04	0.02	0.06	0.01	0.01
Mg	2.52	2.41	0.18	0.05	2.86	2.89	1.30	1.28	0.01	0.01
Al	1.49	1.58	2.33	2.60	2.31	2.26	2.73	2.74	0.00	0.00
Si	6.78	6.69	3.34	3.21	2.91	3.01	2.92	2.85	0.01	0.01
K	0.19	0.21	0.83	0.90	0.02	0.02	0.01	0.02	0.00	0.00
Ca	1.95	1.86	0.01	0.02	0.00	0.01	0.00	0.02	0.96	0.95
Ti	0.17	0.17	0.00	0.02	0.00	0.00	0.00	0.00	0.00	0.00
Cr	0.01	0.00	0.00	0.00	0.01	0.00	0.00	0.00	0.00	0.00
Mn	0.01	0.08	0.00	0.00	0.07	0.00	0.11	0.15	0.01	0.01
Ni	0.00	0.00	0.00	0.00	0.00	0.01	0.00	0.00	0.00	0.00
Fe^{2+}	2.05	2.26	0.21	0.09	1.73	1.66	2.63	2.70	0.00	0.00

For clarity, only two representative analyses of each species are given in this table.
* Total Fe expressed as FeO.

https://doi.org/10.1346/CCMN.2006.0540502 Published online by Cambridge University Press

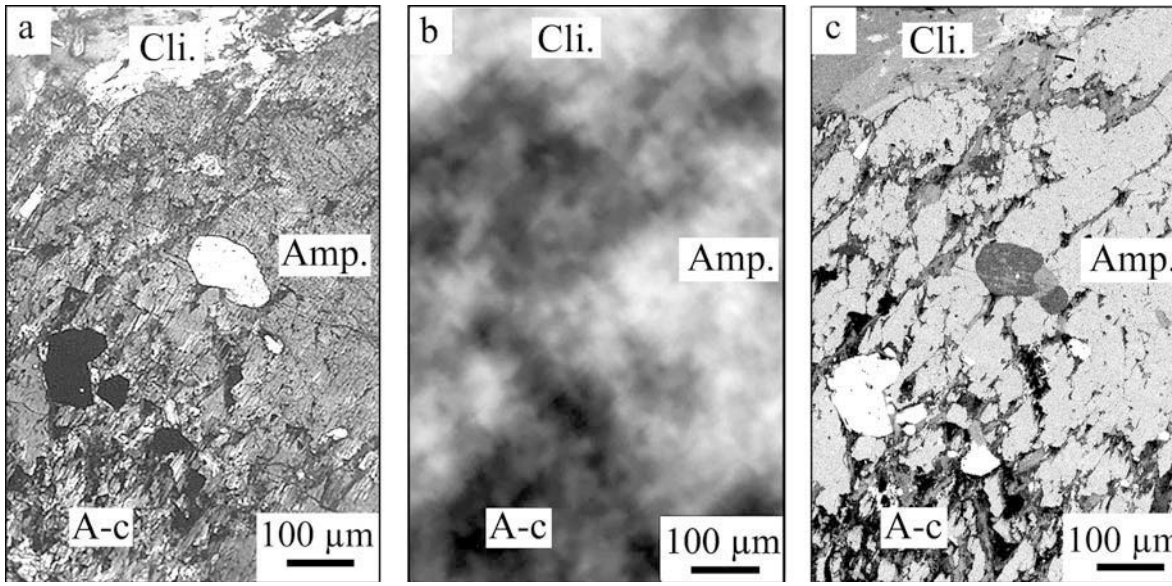

Figure 5. Unaltered granite: (a) image of a partly chlortitized amphibole under plane-polarized light; (b) corresponding autoradiograph; and (c) corresponding backscattered electron image. Amp. = amphibole, Cli. = clinochlore, A-c = amphibole cleavages.

pseudomorphic replacement after amphiboles occurs in non-porous patches (Figure 6b) and the clinochlore to chamosite evolution in the first 4 cm far from the crack implies a large increase in Fe atom content to the detriment of Mg atoms, with a slight increase in Al atoms. In the vicinity of the fracture and up to a depth of 3 cm from the fracture surface in the altered rock, a phengite develops along the amphibole cleavage planes and as intra-mineral microcrack linings. These phengites display (Table 2) high Si-for-Al substitutions in tetrahedral sites (Si atom content ranges from 3.21 to 3.34) and high (Fe+Mg) for Al substitutions in octahedral sites (Fe+Mg atom contents range from 0.14 to 0.39). The location of phengite in microscopic views and in an autoradiograph (Ph. in Figure 6) indicate that phengite replaced an area consisting of porous patches lining the fine amphibole cleavage traces.

Mineralogy and porosity of biotites. Biotites in the unaltered granite appear as large bent flakes up to 2 mm

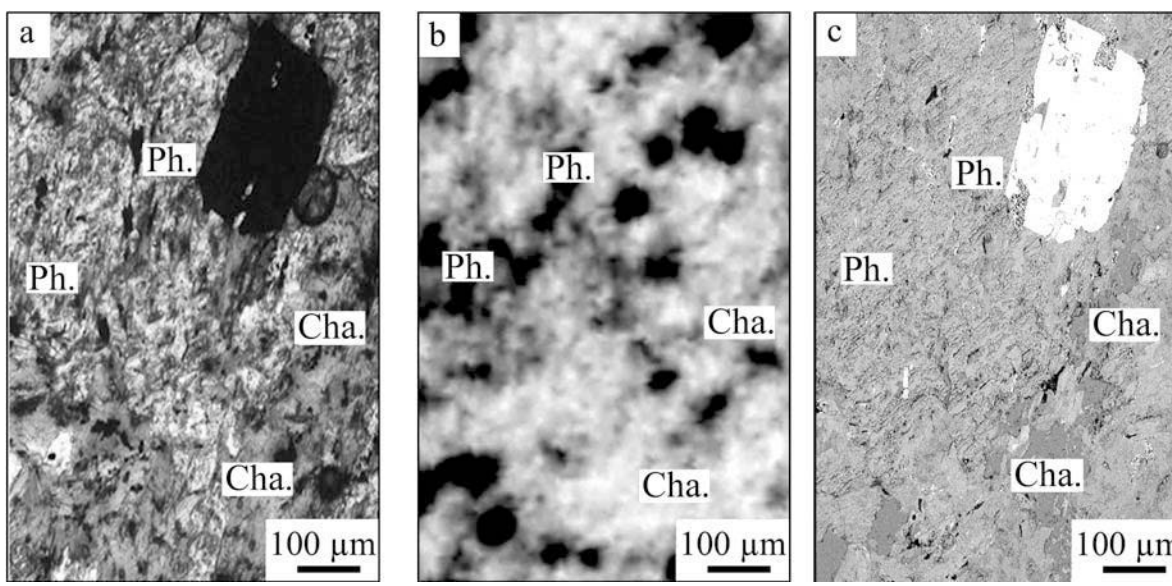

Figure 6. Altered granite: (a) image of totally chloritized and phengitized amphibole under plane-polarized light; (b) corresponding autoradiograph; and (c) corresponding backscattered electron image. Cha. = chamosite, Ph. = phengite.

https://doi.org/10.1346/CCMN.2006.0540502 Published online by Cambridge University Press

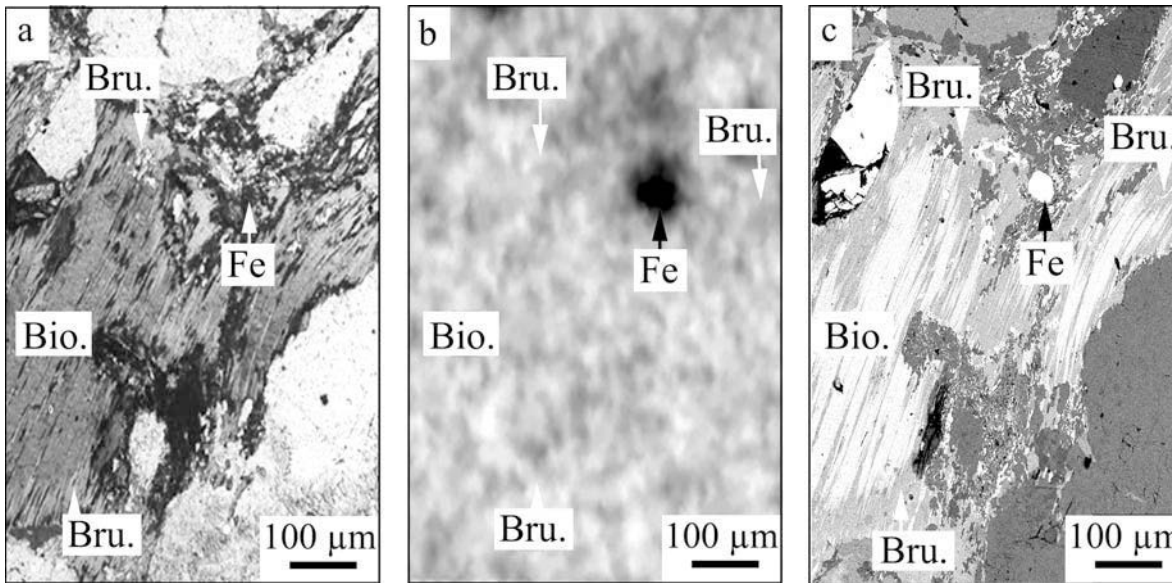

Figure 7. Unaltered granite: (a) image of a partly chloritized biotite under plane-polarized light; (b) corresponding autoradiograph; and (c) corresponding backscattered electron image. Bio. = Biotite, Bru. = Brunsvigite, Fe = Fe oxide.

long with characteristic light- to dark-brown pleochroism under plane-polarized light. Tiny inclusions of euhedral Ti oxides, zircon and apatite crystals are disseminated in the biotite flakes. Smaller biotites also occur as inclusions in amphiboles or filling cracks. The alteration of the biotite begins early in the unaltered granite with its partial pseudomorphic replacement by light-blue chlorite (Bru. in Figure 7a) which does not create significant intragranular porosity as outlined by the white to light gray levels on the autoradiographs (Figure 7b). Some biotite crystals show elongated almond-shaped inclusions of quartz, calcite and K-feldspar and Fe oxide patches (Fe in Figure 7c) which are porous on the autoradiographs (Figure 7b).

The biotites in the altered granite show a general pseudomorphic replacement of the crystal cores by light-blue chlorite (Bru. in Figure 8a) and locally, partial replacement by light-yellow phyllosilicates (Ph. in Figure 8a). X-ray diffraction study of these microsites shows that unaltered biotite is no longer present as indicated by the absence of its characteristic 060 reflection at 1.536 Å (Figure 4b, pattern 4). Biotite

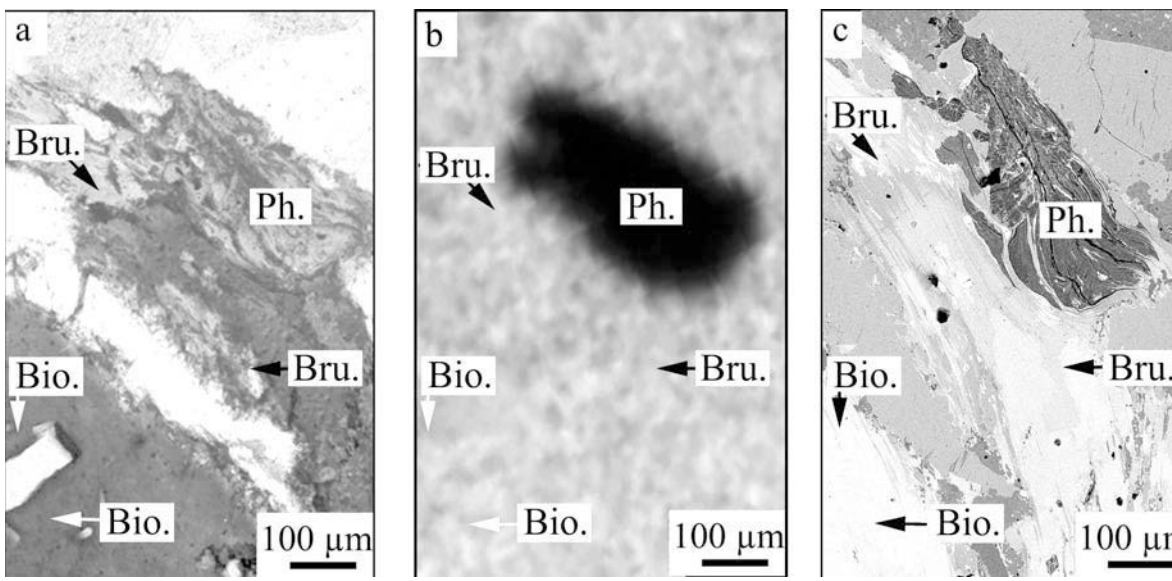

Figure 8. Altered granite: (a) image of chloritized and phengitized biotite under plane-polarized light; (b) corresponding autoradiograph; and (c) corresponding backscattered electron image. Bio. = biotite, Bru. = brunsvigite, Ph. = phengite.

https://doi.org/10.1346/CCMN.2006.0540502 Published online by Cambridge University Press

crystals are replaced by five alteration products (Figure 4b, patterns 1, 2 and 3) including: (a) chlorite with a typical basal reflection series at 14.24, 7.10, 4.72, 3.54 and 2.89–2.84 Å, and the 137 and 060 reflections at 1.573 and 1.549 Å, respectively (ethylene glycol solvation shows no effect); (b) a dioctahedral mica of phengite type with basal reflections at 10.03, 5.01 and 3.33 Å (superimposed on the 3.34 Å quartz reflection), typified by its characteristic dioctahedral 060 reflection at 1.505 Å; (c) trace amounts of calcite revealed by its 3.03 Å reflection (Figure 4b, pattern 1); (d) quartz with 4.26 and 3.34 Å reflections; and (e) orthoclase with its characteristic 002 reflection at 3.25 Å. Apatite revealed by its 2.71 Å reflection was previously observed as a primary inclusion in unaltered biotite, and hence is not included in the alteration products of biotites.

The chemical analyses of biotites (Table 3) support the identification of the alteration minerals by XRD and highlight the chemical evolution of the replacing chlorites with the distance to the fracture surface in the altered granite. The light-blue chlorites observed in unaltered and altered granite as partial or general biotite pseudomorphism give brunsvigite Mg-Fe compositions (Bru. in Figures 7 and 8) with Fe/(Fe+Mg) ratio ranging from 0.42 to 0.50 and Si contents ranging from 2.92 to 3.12 atoms. The light-yellow phyllosilicates observed in altered granite as partial biotite pseudomorphism give phengite compositions with Si contents ranging from 3.27 to 3.30 atoms and Fe+Mg contents ranging from 0.17 to 0.25 atoms. The elongated almond-shaped inclusions yield quartz, calcite and K-feldspar chemical compositions. As the distance to the fracture decreases, the mineralogy, chemistry and spreading of the alteration phases in the altered granite evolves: (1) the Mg-Fe brunsvigite chlorite evolves to Fe-Mg brunsvigite chlorite with Fe enrichment up to 2.60 atoms (Table 3); (2) the quartz, calcite and K-feldspar elongated almonds evolve into dolomite + K-feldspar with the segregation of quartz into individual inclusions; and (3) phengite develops progressively at the expense of biotite, up to the complete crystal pseudomorphosis at the fracture selvage.

The autoradiographs recorded from the biotites in the altered granite (Figure 8b), when compared with the microscopic images (Figure 8a,c), indicate that the chlorites observed as biotite pseudomorphic replacement appear as white to light gray levels and do not present any connected porosity (Bru. in Figure 8b), as already observed in the early stages of biotite alteration (Figure 7b). On the other hand, the phengites observed

Table 3. Chemical composition (wt.%) and structural formulae of biotites and their alteration products.

	Biotite	Biotite	Phengite	Phengite	Mg-Fe brunsvigite	Mg-Fe brunsvigite	Fe-Mg brunsvigite	Fe-Mg brunsvigite	Calcite	Calcite	K-feldspar	K-feldspar
Na_2O	0.07	0.11	0.12	0.14	0.11	0.03	0.02	0.06	0.10	0.04	0.79	0.44
MgO	10.55	10.67	2.12	2.12	14.28	16.05	16.88	11.82	0.37	0.01	0.00	0.02
Al_2O_3	14.82	14.74	27.49	27.84	18.18	18.20	21.17	21.11	0.00	0.02	18.83	19.34
SiO_2	36.94	36.20	50.06	51.40	27.95	28.70	27.55	27.87	0.02	0.51	65.36	65.64
K_2O	9.14	9.40	10.19	10.58	0.04	0.03	0.43	0.12	0.01	0.01	15.42	15.99
CaO	0.00	0.06	0.01	0.10	0.02	0.02	0.00	0.04	58.70	55.36	0.00	0.00
TiO_2	2.94	2.98	1.51	0.61	0.92	0.07	0.00	0.00	0.04	0.00	0.00	0.07
Cr_2O_3	0.00	0.04	0.00	0.00	0.04	0.00	0.00	0.00	0.03	0.00	0.08	0.01
MnO	0.00	0.44	0.00	0.06	0.54	0.17	0.00	0.09	1.10	0.00	0.08	0.00
NiO	0.00	0.13	0.00	0.15	0.05	0.05	0.00	0.00	0.00	0.07	0.16	0.07
FeO*	21.51	21.06	3.67	3.16	21.79	22.21	21.98	30.27	0.31	0.36	0.06	0.05
Total	95.95	95.84	95.15	96.15	83.92	85.53	88.03	91.38	60.69	56.37	100.71	101.62
	11 oxygen basis				14 oxygen basis				1 oxygen basis		8 oxygen basis	
Na	0.01	0.02	0.02	0.02	0.02	0.01	0.00	0.01	0.00	0.00	0.07	0.04
Mg	1.22	1.24	0.21	0.21	2.30	2.53	2.58	1.81	0.01	0.00	0.00	0.00
Al	1.35	1.35	2.18	2.18	2.32	2.27	2.56	2.56	0.00	0.00	1.02	1.03
Si	2.86	2.82	3.36	3.41	3.02	3.04	2.83	2.86	0.00	0.01	2.99	2.98
K	0.90	0.93	0.87	0.90	0.01	0.00	0.06	0.02	0.00	0.00	0.90	0.93
Ca	0.00	0.01	0.00	0.01	0.00	0.00	0.00	0.00	0.97	0.98	0.00	0.00
Ti	0.17	0.17	0.08	0.03	0.07	0.01	0.00	0.00	0.00	0.00	0.00	0.00
Cr	0.00	0.00	0.00	0.00	0.00	0.00	0.00	0.00	0.00	0.00	0.00	0.00
Mn	0.00	0.03	0.00	0.00	0.05	0.02	0.00	0.01	0.01	0.00	0.00	0.00
Ni	0.00	0.01	0.00	0.01	0.00	0.00	0.00	0.00	0.00	0.00	0.01	0.00
Fe^{2+}	1.25	1.24	0.21	0.18	1.97	1.96	1.89	2.60	0.00	0.00	0.00	0.00

For clarity, only two representative analyses of each species are given in this table.
* Total Fe expressed as FeO.

https://doi.org/10.1346/CCMN.2006.0540502 Published online by Cambridge University Press

as partial biotite pseudomorphism appear as black patches on autoradiographs (Ph. in Figure 8b) which are indicative of highly connected porosity. Similar porosity is observed for the quartz + calcite + K-feldspar inclusions. Additional minor porous inclusions are observed in the biotites in the vicinity of the fracture, with calcite + K-feldspar and quartz crystallizations, respectively.

As previously observed in the mineralogical study, the phengites develop progressively at the expense of biotite, up to the complete crystal pseudomorphosis at the fracture selvage. Study of the autoradiographs indicates that this phengitization process creates connected porosity in the biotite crystals, as already observed in the amphibole crystals.

Mineralogy and porosity of plagioclases. The plagioclases observed in the unaltered granite appear as subhedral phenocrysts up to 1 cm long with polysynthetic twinnings and zoning. Their chemical composition corresponds to $An_{31}-An_{32}$ (Table 4). The connected porosity oberved on the plagioclase autoradiograph is only located in microcracks and grain boundaries. Some andesine crystals are partly albitized but the albitized zones are not connected to the porous network. The albitization process in the altered granite results in complete albite-for-andesine replacement. The albitization is exemplified by XRD patterns for powder, air-dried and ethylene glycol-solvated samples recorded from altered microsampled plagioclases (Figure 4c). The dominant feldspar on XRD patterns is albite with a characteristic 002 reflection at 3.19 Å associated with additional reflections at 6.39, 4.04, 3.77, 3.76, 2.97, 2.94 and 2.86 Å. Another alteration feature affects the plagioclases close to the fracture in the form of albite corrosion with crystallization of secondary micas (up to 0.1 mm) that are uncolored under plane-polarized light and bright blue to yellow under crossed nicols (Figure 9a). This secondary mica is a dioctahedral phengite with basal reflections at 10.07, 4.99 and 3.34 Å. Trace amounts of Fe-chlorite are detected by a 002 reflection at 7.07 Å and a 004 reflection at 3.50 Å (Figure 4c). This alteration results in the development of porous patches in the core of the non fractured feldspars which increase the connected porosity drastically (Figure 9b,c). The evolution of the mineralogy and the porosity as a function of fracture distance is in good agreement with the three alteration zones revealed by the plagioclase staining colors within the mineralogical map (Figure 2b,c).

These results clearly demonstrate that the connected porosity created in a given rock by the alteration process is controlled for the most part by the nature of the rock-forming minerals and their alteration phases. The

Table 4. Chemical composition (wt.%) and structural formulae of plagioclases and their alteration products.

	Plagioclase	Plagioclase	Albite	Albite	Phengite	Phengite
Na_2O	8.32	8.09	10.79	10.75	0.16	0.18
MgO	0.01	0.00	0.09	0.05	0.74	1.09
Al_2O_3	24.98	25.83	21.38	20.74	30.10	29.83
SiO_2	60.79	60.40	66.38	67.75	48.58	50.01
K_2O	0.15	0.08	0.79	0.25	9.93	9.93
CaO	6.75	6.86	0.41	0.24	0.00	0.12
TiO_2	0.01	0.07	0.08	0.00	0.13	0.20
Cr_2O_3	0.00	0.00	0.00	0.04	0.00	0.06
MnO	0.19	0.00	0.00	0.01	0.08	0.04
NiO	0.00	0.00	0.00	0.00	0.11	0.00
FeO*	0.00	0.00	0.30	0.32	5.19	5.32
Total	101.20	101.33	100.46	100.15	95.02	96.77
	— 8 oxygen basis —		— 8 oxygen basis —		— 11 oxygen basis —	
Na	0.71	0.69	0.92	0.91	0.02	0.02
Mg	0.00	0.00	0.01	0.00	0.07	0.11
Al	1.30	1.34	1.10	1.07	2.40	2.33
Si	2.68	2.66	2.91	2.96	3.29	3.32
K	0.01	0.00	0.04	0.01	0.86	0.84
Ca	0.32	0.32	0.02	0.01	0.00	0.01
Ti	0.00	0.00	0.00	0.00	0.01	0.01
Cr	0.00	0.00	0.00	0.00	0.00	0.00
Mn	0.01	0.00	0.00	0.00	0.00	0.00
Ni	0.00	0.00	0.00	0.00	0.01	0.00
Fe^{2+}	0.00	0.00	0.01	0.01	0.29	0.30

For clarity, only two representative analyses of each species are given in this table.
* Total Fe expressed as FeO.

https://doi.org/10.1346/CCMN.2006.0540502 Published online by Cambridge University Press

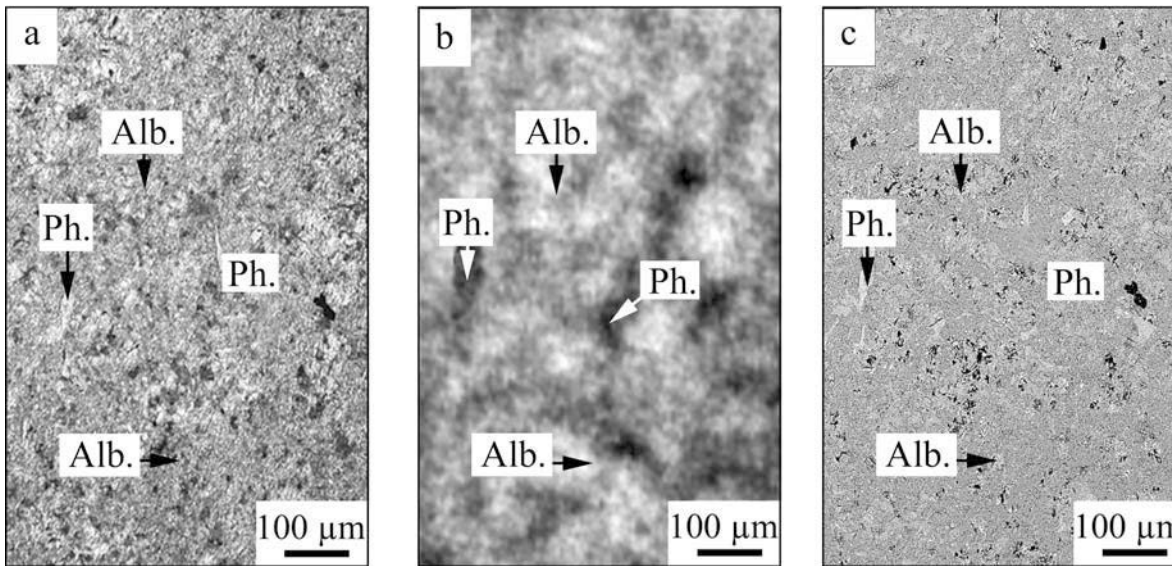

Figure 9. Altered granite: (a) image of totally albitized and phengitized plagioclase under plane-polarized light; (b) corresponding autoradiograph and (c) corresponding backscattered electron image. Alb. = albite, Ph. = phengite.

primary ferromagnesian minerals, much more sensitive to alteration than feldspars and quartz, are the major mineral species which account for the bulk porosity increase observed in the altered granite. However, this bulk connected porosity is at the same time influenced by the nature of the neoformed phases which replaced each primary mineral species. The microscopic study of these minerals, when correlated to autoradiographs, indicates that the general chloritization of the ferromagnesian minerals as well as the albitization of the feldspars do not create connected porosity. On the other hand, the pervasive phengitization which develops in the ferromagnesian minerals and feldspars within altered granite appears as the major alteration process for connected porosity creation within the studied granite.

DISCUSSION

This integrated study which links the porosity and the mineralogical heterogeneity of a rock from core to mineral scale reveals that porosity increases more than four times from the unaltered to the altered rock. Although this increase in porosity has already been observed in previous studies (Sammartino, 1998; Sausse *et al.*, 2001; Schild *et al.*, 2001; Siitari-Kauppi, 2002; Ota *et al.*, 2003), the present study pinpoints the location of porosity development, in a fracture-free sample, thus demonstrating that the porosity increase originates from the rock fabric itself (*i.e.* the geometrical organization and relationships of mineral grains and microcracks that control matrix porosity). This association of mineralogical and porosity studies at the micrometer scale helps to reveal the influence of alteration processes upon fluid circulation in the rock matrix.

As a first important result, it has been shown that the connected matrix porosity which develops in the course of rock alteration could be considered as a collection of interconnected particular porous microsites which have specific features according to the rock-forming minerals concerned. The cleavage pattern of the amphibole crystals favors the development of a connected porosity network, mainly by submicroscopic cleavages opening (apertures measured from 0.1 µm to 2.5 µm) yielding a mineral-specific porosity greater than in quartz and feldspars. Biotite crystals exhibit a different connected porosity pattern with only open grain boundaries and no intragranular cracks nor cleavage openings. The total amount of connected porosity of ferromagnesian (biotite and hornblende) minerals in unaltered granite is greater (0.4%) than the other minerals (Table 1).

The ferromagnesian minerals are the most porous mineral group whatever the degree of alteration, but the proportion of the porosity due to amphibole and biotite and the way it develops (from 0.4 to 3.7%) differs. The connected porosity which develops inside the amphibole depends on the nature and crystallization microsites of their alteration products. Chloritization affecting the amphibole crystals is the major process which develops with alteration. Two chemically distinct chlorites are produced, *i.e.* Mg-clinochlore in the altered granite far from the fracture and Fe-chamosite in its vicinity. Whatever the chemistry of the chlorites, these minerals do not show any connected porosity and, as a consequence, amphibole cores remain unporous. As shown by SEM and autoradiograph observations, the development of the connected amphibole porosity in the selvage of the fracture results from phengite crystallization within the cleavages opened through amphibole dissolution. These phengites are porous minerals which,

https://doi.org/10.1346/CCMN.2006.0540502 Published online by Cambridge University Press

unlike chlorite pseudomorphs, do not seal the connected porosity. The development of connected porosity in biotite with alteration is the result of three different processes which can be observed in the same crystal: (1) 'sealing pseudomorphism' with non-porous chlorite for biotite replacement, in a similar way to amphibole; (2) 'open pseudomorphism' with porous phengite for biotite replacement in the vicinity of the fracture; (3) porous crystallization of quartz + calcite + K-feldspar assemblage as almond-shaped inclusions differentiating into porous calcite + K-feldspar and non-porous quartz inclusions in the vicinity of the fracture.

As a second result, it has been shown that these primary minerals, which have their specific crystallochemistry and their own connected porosity patterns, produce specific alteration phases which, in turn, have their own porosity properties and, hence, will control the rock matrix porosity development, as shown in the altered granite. The porosity network of quartz and K-feldspars does not change with alteration and remains constituted by microcracks and open grain boundaries yielding porosity values similar to those for the unaltered rock (overestimated value of 0.80% for quartz and 0.30% for K-feldspars) with no observable alteration phases. The alteration of plagioclases develops connected pores constituted by open grain boundaries and microcracks. The albitization process develops in the altered granite (up to the complete replacement of andesine by albite), but without increase in the connected porosity, except when patches connect to an open grain boundary or an open microcrack. This last process can be suggested to explain the formation of the alteration zones 3 and 2 (Figure 2c), proven by the staining colors of the plagioclases, and typified by the progressive rock porosity increase from 0.7% to 1.6%, respectively. The phengitization process affects the plagioclases in the vicinity of the fracture to form a porous habit (SEM observation) in the albitized patches. This leads to the formation of the alteration zone 1 (Figure 2c), closest to the fracture surface with a rock porosity reaching 3.7%.

These results are a representative part of larger work including the study of several igneous rock types such as tonalite, leucogranite and monzodiorite. This integrated work coupling porosity and mineralogy studies is applied in this paper to the propylitic alteration which is one of the most ubiquitous processes affecting igneous rocks, but it could be applied to any other petrographic study dealing with alteration processes. In particular, it could be useful for the assessment of a radioactive waste repository in a granitic environment where the connected porosity of the host rock is the major parameter controlling migration of radionuclides through the geosphere. Another major application could be the calculation of geochemical mass balances in rock weathering or hydrothermal alteration using a map of alteration phases (alteration phases and element-distribution mapping obtained using SEM) for each kind of primary mineral at the microscopic scale.

CONCLUSIONS

Mineralogical and porosity data demonstrate that the location and the development of the fluid circulation pathways in a given rock are strongly dependent on: (1) the crystallochemistry of the rock-forming minerals; (2) the geometrical organization and development of alteration microsites in these minerals (pseudomorphosis and/or internal microcracks); and (3) the crystallochemistry of the alteration products. As a consequence, porosity studies of rock alteration have to take into account these structural, geometrical and mineralogical heterogeneities of alteration products at microscopic scale to estimate the actual permability of a given rock and its potential evolution in the course of alteration.

ACKNOWLEDGMENTS

The authors acknowledge the thorough reviews of Dr Ray Ferrell and Dr Paul Schroeder. Financial support for this research was provided by ANDRA (French National Agency for Nuclear Waste Storage).

REFERENCES

Bertrand, J.M., Leterrier, J., Cuney, M., Brouand, M., Stussi, J.M., Delaperrière, E. and Virlojeux, D. (2001) Géochronologie U-Pb sur zircons de granitoïdes du Confolentais, du massif de Charroux-Civray (Seuil du Poitou) et de Vendée. *Géologie de la France*, **1-2**, 167–189.

David, F. and Walker, L. (1990) Ion microprobe study of intragrain micropermeability in alkali feldspars. *Contributions to Mineralogy and Petrology*, **106**, 124–128.

Duliu, O. G. (1999) Computer axial tomography in geosciences: an overview. *Earth-Science Reviews*, **48**, 265–281.

Ferry, J.M. (2000) Patterns of mineral occurence in metamorphic rocks from the Isle of Skye, Northwest Scotland. I: granites. *Contributions to Mineralogy and Petrology*, **91**, 283–304.

Fredrich, J.T. and Lindquist, W.B. (1997) Statistical characterization of the three-dimensional microgeometry of porous media and correlation with macroscopic transport properties. *International Journal of Rock Mechanics and Mining Sciences*, **34**, 3–4.

Freiberger, R. (2000) P-T-X conditions of the late magmatic to early postmagmatic crystallization history of intermediate to basic plutonites: The Hercynian granitoid complex of Charroux-Civray, NW border of the Massif Central, France. Thesis, University of Munich, Germany, 204 pp.

Geraud, Y., Mazerolle, F. and Raynaud, S. (1992) Comparison between connected and overall porosity of thermally stressed granite. *Journal of Structural Geology*, **14**, 981–990.

Geraud, Y., Mazerolle, F., Raynaud, S. and Lebon, P. (1998) Crack location in granitic samples submitted to heating, low confining pressure and axial loading. *Geophysical Journal International*, **133**, 553–567.

Hellmuth, K.H., Siitari-Kauppi, M. and Lindberg, A. (1993) Study of porosity and migration pathways in crystalline rock by impregnation with ^{14}C-polymethylmethacrylate. *Journal of Contaminant Hydrology*, **13**, 403–418.

Hellmuth, K.H., Lukkarinen, S. and Siitari-Kauppi, M. (1994) Rock matrix studies with carbon 14-polymethylmethacrylate (PMMA); method development and applications. *Isotopenpraxis, Environmental and Health Studies*, **30**, 47–60.

Hellmuth, K.H., Siitari-Kauppi, M., Klobes, P., Meyer, K. and Goebbels, J. (1999) Imaging and analyzing rock porosity by autoradiography and Hg-porosimetry/X-ray computertomography – applications. *Physics and Chemistry of the Earth*, **24**, 569–573.

Karacan, C.O., Grader, A.S. and Halleck, P.M. (2003) Evaluation of local porosity changes in limestone samples under triaxial stress field by using X-ray computed tomography. Pp. 177–189 in: *Applications of X-ray Computed Tomography in the Geosciences* (F. Mees, R. Swennen, M. van Geet and P. Jacobs, editors). Special Publication, **215**, Geological Society, London.

Leake, B.E. and co-authors (IMA) (1978) Nomenclature of amphiboles. *Mineralogical Magazine*, **42**, 533–563.

Melnyk, T.W. and Skeet, A.M.M. (1986) An improved technique for the determination of rock porosity. *Canadian Journal of Earth Science*, **23**, 1068–1074.

Montgomery, C.W. and Brace, W.F. (1975) Micropores in plagioclase. *Contributions to Mineralogy and Petrology*, **52**, 17–28.

Montoto, M., Martinez-Nistal, A., Rodriguez-Rey, A., Fernandez-Merayo, N. and Soriano, P. (1995) Microfractography of granitic rocks under confocal scanning laser microscopy. *Journal of Microscopy*, **177**, 138–149.

Müller, G. (1967) *Methods in Sedimentary Petrology*. Hafner Publication Company, New York, 283 pp.

Ota, K., Mori, A., Alexander, W.R., Frieg, B. and Schild, M. (2003) Influence of the mode of matrix porosity determination on matrix diffusion calculations. *Journal of Contaminant Hydrology*, **61**, 131–145.

Putnis, A. (2002) Mineral replacement reactions: from macroscopic observations to microscopic mechanisms. *Mineralogical Magazine*, **66**, 689–708.

Revil, A. and Glover, P.W.J. (1997) Theory of ionic surface electrical conduction in porous media. *Physical Review B*, **55,** 1757–1773.

Sammartino, S. (1998) La caractérisation d'un matériau à faible perméabilité: mesures expérimentales et analyse d'images: application à la tonalite du sud Vienne, effet de l'altération. Thesis University of Poitiers, France, 152 pp.

Sardini, P., Moreau, E., Sammartino, S. and Touchard, G. (1999) Primary mineral connectivity of polyphasic igneous rocks by high-quality digitisation and 2D image analysis. *Computers and Geosciences*, **25**, 599–608.

Sausse, J., Jacquot, E., Fritz, B., Leroy, J. and Lespinasse, M. (2001) Evolution of crack permeability during fluid-rock interaction. Example of the Brézouard granite (Vosges, France). *Tectonophysics*, **336**, 199–214.

Schild, M., Siegesmund, S., Vollbrecht, A. and Mazurech, M. (2001) Characterization of granite matrix porosity and pore-space geometry by in-situ and laboratory methods. *Geophysical Journal International*, **146**, 111–125.

Siitari-Kauppi, M. (2002) Development of ^{14}C-polymethylmethacrylate method for the characterisation of low porosity media. Thesis, University of Helsinki, 156 pp.

Siitari-Kauppi, M., Flitsiyan, E.S., Klobes, P., Meyer, K. and Hellmuth, K.H. (1998) Progress in physical rock matrix characterization: structure of the pore space. *Materials Research Society*, **506**, 671–678.

Suzuki, K., Oda, M., Yamakasis, M. and Kuwahara, T. (1998) Permeability changes in granite with cracks during immersion in hot water. *International Journal of Rock Mechanics and Mining Sciences*, **35**, 907–921.

Vaughan, P.J., Moore, D.E., Morrow, C.A. and Byerlee, J.D. (1986) Role of cracks in progressive permeability reduction during flow of heated aqueous fluids through granite. *Journal of Geophysical Research*, **91**, 7517–7530.

Walker, F.D.L., Lee, M.R. and Parsons, I. (1995) Micropores and micropermeable texture in alkali feldspars: geochemical and geophysical implications. *Mineralogical Magazine*, **59**, 507–536.

(*Received 22 December 2005; revised 10 May 2006; Ms. 1125; A.E. Ray E. Ferrell Jr.*)